Colloids and Surfaces B: Biointerfaces 214 (2022) 112462

Contents lists available at ScienceDirect

Colloids and Surfaces B: Biointerfaces

journal homepage: www.elsevier.com/locate/colsurfb

MoS_2/LaF_3 for enhanced photothermal therapy performance of poorly-differentiated hepatoma

Lin Sun [a], Huifang Bai [b], Hanjin Jiang [c], Peng Zhang [a,e], Jian Li [b], Weidong Qiao [b], Dong Wang [c], Guosong Liu [d], Xuelin Wang [b,*]

[a] College of Chemistry, Jilin University, Changchun 130012, PR China
[b] Key Laboratory of Zoonosis Research, Ministry of Education, Institute of Zoonosis, College of Veterinary Medicine, Jilin University, Changchun 130062, PR China
[c] College of Chemical Engineering, Northeast Electric Power University, Jilin City 132012, PR China
[d] Changchun Institute of Optics Fine Mechanics and Physics, Chinese Academy of Sciences, Changchun 130033, PR China
[e] Electron microscope center, Jilin University, Changchun 130012, PR China

ARTICLE INFO

Keywords:
MoS_2 nanoflowers
LaF_3 nanoparticle
Photothermal therapy
PTT
Antitumor treatment

ABSTRACT

Photothermal therapy (PTT) based on nanoparticle had been widely used to antitumor treatment. However, low photothermal conversion efficiency (PCE) is the main hurdle for antitumor treatment. To improve the PCE and gain ideal clinical the nanoparticle with higher photothermal conversion efficiency, we have developed a highly efficient solar absorber with MoS_2/LaF_3/ polydimethylsiloxane(PDMS) which can enhance the absorption of solar irradiation engergy, however, its photothermal effect irradiated by near-infrared light has not yet been investigated. The knowledge absence in photothermal effect will impede MoS_2/LaF_3/PDMS to be used for cancer therapy in clinic. In this study, we applied LaF_3-loaded, MoS_2-based photothermal conversion agents (PTAs) for improved photothermal cancer therapy. The study showed that the MoS_2/LaF_3 nanoflowers showed higher photothermal conversion efficiency (PCE, 42.5%) and could more effectively inhibit cancer cell proliferation compared to MoS_2-based PTT agents *in vitro*. *In vivo*, the results further revealed that photothermal therapy using MoS_2/LaF_3 nanoflowers could significantly inhibit solid tumor growth. The study clearly demonstrated that MoS_2/LaF_3 could work at under low power NIR Laser *in vitro* and *in vivo*, resulting in a very impressive therapeutic effect in tumor-bearing mice. The MoS_2/LaF_3 nanoflowers will be prominent candidate nanoparticle for effective inhibiting tumor growth by photothermal therapy.

1. Introduction

Cancer therapy is still facing an ordeal challenge in worldwide. Although cancer classical therapies, including chemotherapy, surgery and radiotherapy are available, these treatments have been impeded by serious side effects on immune system and bone marrow hematopoietic function [1–4]. Recently, photothermal therapy (PTT) with a new minimally invasive therapy and low side effects has attracted much attention in matching classical therapy of cancer [5–7]. The studies had demonstrated that photothermal conversion agents (PTAs) can kill tumor cell by converting the absorbed near-infrared (NIR) light into heat and producing localized hyperthermia to antitumor *in vitro* and *vivo* [8–15]. As one of a focused nanomaterials with strong NIR photothermal absorption, excellent stability and biocompatibility, molybdenum disulfide(MoS_2) nanosheets with a smaller size and PEGylation modification has showed enhanced photothermal conversion efficiency and used as PTAs MoS_2. However, low photothermal conversion efficiency (PCE) is the main hurdle for MoS_2-based PTAs [16–21]. To improve the PCE, nanoparticle modification, such as plasmic noble metals, polymers and semiconductors have been used as surface modification materials of the MoS_2-based PTAs [21–24]. Among these various compositions, the integration of semiconductors with plasmic noble metals could significantly enhance light absorption capacity and amplify its optical and electrical performance [25–31].

We have developed a highly efficient solar absorber with MoS_2/LaF_3/ polydimethylsiloxane(PDMS) [32]. The evaporation rate of the solar evaporation device was 1.76 kg m^{-2} h^{-1} under the solar irradiation of 0.1 W cm^{-2}. We demonstrated that the combination of solid electrolyte and semiconductor could improve the solar light absorption capacity and light-to-heat conversion capacity of the material [32].

* Corresponding author.
E-mail address: xuelin@jlu.edu.cn (X. Wang).

https://doi.org/10.1016/j.colsurfb.2022.112462
Received 14 November 2021; Received in revised form 2 March 2022; Accepted 11 March 2022
Available online 16 March 2022

MoS_2/LaF_3/PDMS can enhance the absorption of solar irradiation engergy, however, its photothermal effect irradiated by near-infrared light has not yet been investigated. The knowledge absence in photothermal effect will impede MoS_2/LaF_3/PDMS to be used for cancer therapy in clinic. In this study, we applied LaF_3-loaded, MoS_2-based PTAs for improved photothermal cancer therapy. The LaF_3-loaded MoS_2 nanoflowers showed enhanced photocytotoxicity of cancer cells *in vitro* as compared to MoS_2 nanoparticle. Furthermore, PTT results *in vivo* antitumor efficacy confirmed the great therapeutic potential of MoS_2/LaF_3. Therefore, our study clearly demonstrated that MoS_2/LaF_3 could work at under low power NIR Laser *in vitro* and *in vivo*, resulting in a very impressive therapeutic effect in tumor-bearing mice. The experimental process was illustrated in Scheme 1.

2. Experimental section

2.1. Materials

Lanthanumnitrate ($La(NO_3)_3{\cdot}nH_2O$), Polyvinylpyrrolidone (K30) and Molybdenum (VI) dioxide bis(acetylacetonate) ($C_{10}H_{14}MoO_6$) were purchased from DingGuo Biotechnology Co., Ltd. D-Cysteine (99.0%), 3-(4, 5- Dimethylthiazol- 2-yl)- 2, 5-diphenyltetrazolium bromide (MTT) were bought from Sigma-Aldrich Inc. Penicillin (100 IU/mL) and streptomycin (100 IU/mL), Calcein-AM/PI Double Staining Kit, RPMI-1640 cell culture medium and Fetal Bovine Serum (FBS) were from Gibco. Hela cervical cancer and H22 hepatoma cell line were purchased from Bio-Rad Life Sciences Development Co. Ltd. (Beijing, China). 6–8 week female BALB/c mice with certificate No. 2016–0001 in conformity with SCXK were purchased from Experimental Animal Center, Medical College of Norman Bethune (Changchun, China).

2.2. Synthesis of the LaF_3 nanoparticle

Both 1.2 mmol La $(NO_3)_3$ and 0.778 μg polyvinylpyrrolidone (K30) were put into 18 mL ethylene glycol. Then, 3.6 mmol of NH4F solved in 12 mL of ethylene glycol with stirring for 0.5 h. After continuously stirring, the formed mixture was removed into a stainless steel reactor and sealed tightly at 200 °C for 2 h. The suspensions were purified by centrifugation and dispersed in ethanol. For the preparation of MoS_2/LaF_3 nanoflowers, 0.088 mol of LaF_3 nanoparticle was solved in 30 mL water and mixed with 8 mmol of D-Cysteine. 4 mmol of $C_{10}H_{14}MoO_6$ and 1 mL of Hexamethylene imine were dissolved in 30 mL ethyl acetate. Then, the two solutions were mixed and placed in the stainless steel reaction kettle at 180 °C overnight. The nanocomposite was purified with DI water and ethanol.

2.3. Characterization

The final product was evaluated with Bruker D8 Advance XRD. SEM pictures weregotten by an FEI Tecnai G2-Twin electron microscope. TEM images were gained by a JEM-2100 F electron microscope. The UV-Vis-NIR spectra were tested by a Shimadzu UV-2550. The Raman measurements were performed by the HORIBA T64000.

2.4. Photothermal conversion properties test

To explore the photothermal effects, MoS_2/LaF_3 nanoflowers with different concentrations were measured by laser irradiation (808 nm NIR, 1.2 W cm^{-2}). The photostability of MoS_2/LaF_3 nanoflowers was examined for five laser on-off cycles. The volume for each experiment was 500 μL. The PCE was calculated by the equation as follows:

$$\eta=[hS(T_{max}-T_{surr})-Q_0]/[I(1-10^{-A})]^{37}$$

In equation, S is the surface area and h is the heat transfer coefficient. T_{max} is the equilibrium maximum temperature, T_{surr} is the surrounding temperature. Q_0 is the heat absorption of water; I is the laser power density (1.2 W cm^{-2}), and A is the optical density of MoS_2/LaF_3 nanoflowers at 808 nm.

2.5. Hemolysis test

Fresh red blood cells (RBCs) were kept in a venous blood specimen collection test tube. RBCs were washed with PBS several times *via* at 2500 rpm for 10 min. The RBCs were diluted in PBS buffer (1:10 V/V). Then, 200 μL of diluted whole blood was mixed with 800 μL of the

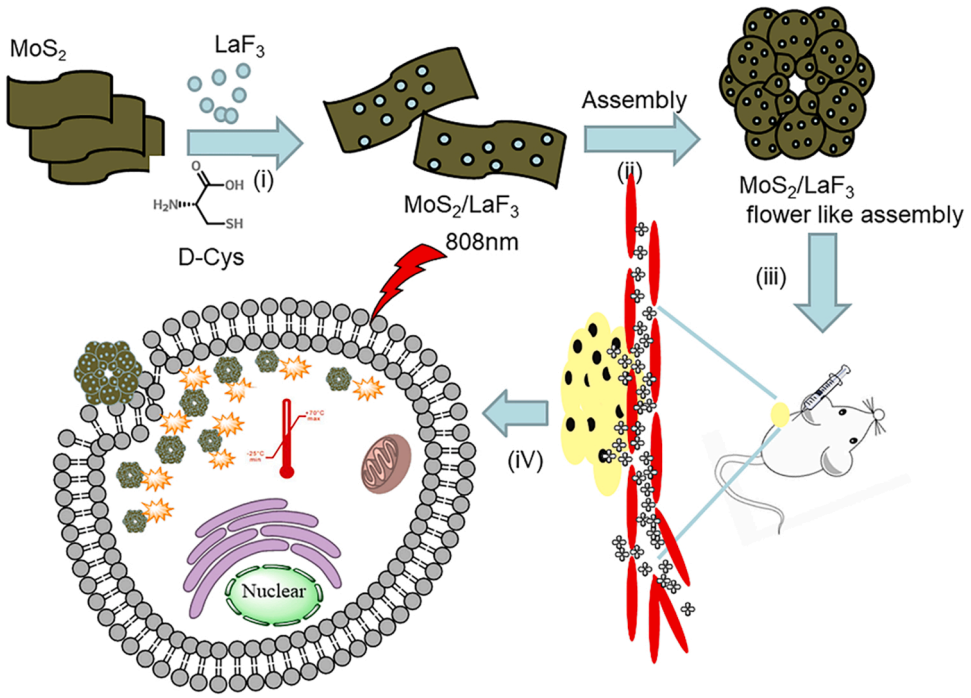

Scheme 1. Scheme representation of the construction of LaF_3 nanoparticle decorated MoS_2 nanoflowers as a NIR photothermal therapy.

sample solution and incubated for 3 h. The deionized water mixture was positive control, and the PBS buffer mixture was negative control. Afterward, all samples were isolated at 2500 rpm for 10 min, and then, the supernatants were tested at 516 nm by an automatic microplate absorbance reader. The hemolysis ratio was recorded as the following equation:

Hemolytic rate $= (OD_{sample}\text{-}OD_{negative\ sample})/(OD_{positve\ sample}\text{-}OD_{negative\ sample}) \times 100\%$ [33].

2.6. In vitro cytotoxicity detection

MTT was used to quantitative analysis the cytotoxicity of MoS_2/LaF_3 nanoflowers and its phototherapy antitumor effect. Cancer cells (Hela cell line) seeded into 96-well and cultured for 24 h. The medium was replaced with fresh culture medium containing serial concentrations of MoS_2/LaF_3 nanoflowers were added into each well. For phototherapy antitumor test, the cells were treated by 808 nm NIR for 5 min (1.2 W cm^{-2}), these cells were cultured for 24 h and then added by 20 μL of MTT (5 mg/mL) in PBS. The cells were further incubated for 4 h and generated MTT formazan. The formazan crystals in 96-well were dissolved in DMSO (150 μL) for 15 min. The samples were determined at 610 nm on a microplate absorbance reader.

To further study the PTT effect of MoS_2/LaF_3 nanoflowers on tumor cell, Fluorescence staining observation was carried out using Calcein-AM/PI kit. Hela cells at a density of 1×10^5 were seeded into 24-well plate. Different concentrations MoS_2/LaF_3 nanoflowers dispersed in RPMI-1640 was cocultured with cells for 6 h. Then, the NIR irradiation (1.2 W cm^{-2}) was conducted on cells for 5 min. For Calcein-AM/PI imaging, the samples were isolated and tested with a calcein-AM/PI kit. Fluorescent images were taken by confocal microscope.

2.7. Photothermal therapy in vivo

H22 hepatocellular carcinoma cells were harvested and resuspended in the PBS. H22 hepatocarcinoma cells (1×10^6 cells per mouse) was injected on BALB/c mice by subcutaneous injection. When the tumor size reached ~350 mm^3, tumor-bearing mice were separated into four groups (n = 4): PBS group, PBS with irradiation group, MoS_2/LaF_3 nanoflowers group and MoS_2/LaF_3 nanoflowers with irradiation group (808 nm, 1.2 W cm^{-2},10 min) were injected subcutaneously with the dosage of a 250 μg mL^{-1}. Thermal imaging was monitored by Fluke-Ti10. Volume (mm^3) = (L*W^2)* 0.5 (L and W defined the length and width, respectively) tumors were measured every two days after irradiation. The BALB/c mice were euthanized at the end of two weeks. The tumors and the major organs were excised and sliced for histology research.

3. Results and discussions

3.1. Synthesis and characterization

Scheme 1 demonstrated the synthesis of MoS_2/LaF_3 nanoflowers as a NIR photothermal agent for antitumor. (i, ii) Self-assembly of MoS_2 with LaF_3 nanoparticle hierarchical nanostructure. (iii) injection of the MoS_2/LaF_3 nanoflowers to the tumor. (iv) NIR-trigged antitumor phototherapy *in vivo*.

TEM observations showed the morphology and structure of the nanocomposite. Ultrathin MoS_2/LaF_3 nanoflowers were overlapped and curled (Fig. 1a). Fig. 1b showed that the LaF_3 nanoparticle was modified on a thin MoS_2 layer and looked blurred and dark. From Fig. 1c, the lattice fringes of MoS_2 nanosheet and LaF_3 nanoparticle could be observed. LaF_3 exhibited an interlayer distance of (113) planes of 0.251 nm and (220) planes of 0.273 nm. These results revealed a well-defined crystal structure, suggesting that the decoration of LaF_3 nanoparticle on the surface of MoS_2 nanosheet.

SEM result confirmed that MoS_2/LaF_3 nanoflowers had hierarchical flowerlike structures (Fig. 2a-b). The nanoflowers presented a nanoflakes assembly structure in the range of 310 − 810 nm size diameter and assembling to form clusters. The magnification view in Fig. 1b showed that the hierarchical nanoflower consisted of ultrathin nanoflakes that thickness was less than 12 nm. XRD result in Fig. S1 indicated successful synthesis crystalline structure of MoS_2/LaF_3 nanoflowers. The characteristic peaks of sample LaF_3 at the as-prepared showed diffraction peaks at 27.511 and 44.747 matched with (113) and (111) of a hexagonal LaF_3 (JCPDS 32–0483). No other impurity peaks were observed. Simultaneously, two diffraction peaks of layer-expanded MoS_2 appeared in the low-angle region corresponding to the (001) and (002) reflections. From the Raman spectra of MoS_2, one characteristic Raman peak of 376 cm^{-1} was observed. The peak corresponded to the E^1_2 g modes of 2 H-MoS_2, which was indicated as an opposite vibration between two S atoms and one Mo atom [34]. No shift was observed in Raman spectra of MoS_2/LaF_3 nanoflowers (Fig. S2). In the UV−vis spectrum (Fig. 3a), MoS_2/LaF_3 nanoflowers also displayed the same absorption peak of MoS_2. These results indicated that LaF_3 deposition did not alter the crystal phase of the MoS_2 nanoflowers, such assembled structures enhanced NIR absorbance, because of the increase in optical path length and the improvement irradiation time.

3.2. Photothermal conversion effect

To investigate the photothermal effect of MoS_2/LaF_3 nanoflowers *in vitro*, MoS_2/LaF_3 nanoflowers at different concentrations (0 −1 mg/mL) were subjected to 808 nm irradiation at 1.2 W cm^{-2} for 300 s. In contrast to the water control, MoS_2/LaF_3 nanoflowers concentration varied from 31.25 to 1000 μg/mL. Its maximum temperature increased

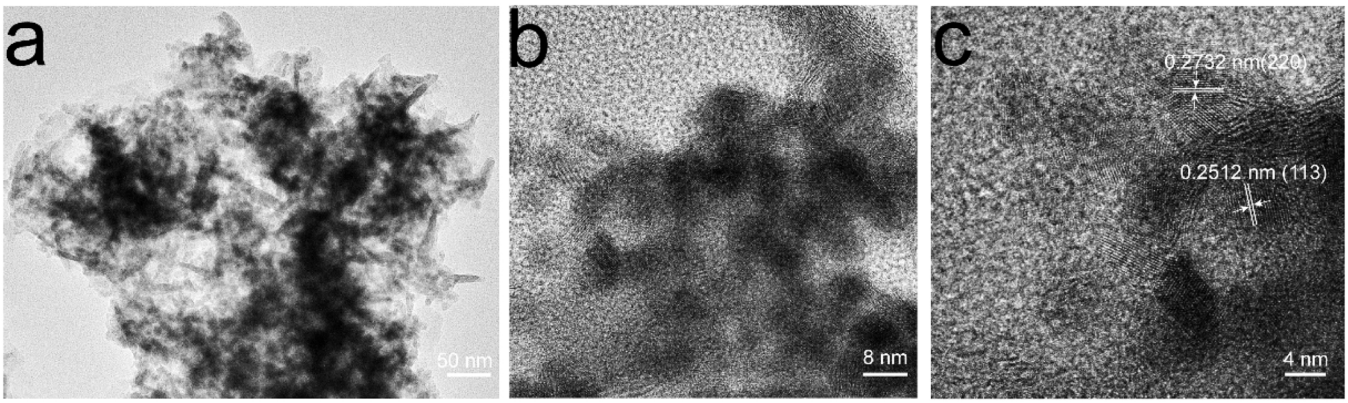

Fig. 1. Typical TEM image(a) and HRTEM image of MoS_2/LaF_3 nanoflowers(b-c).

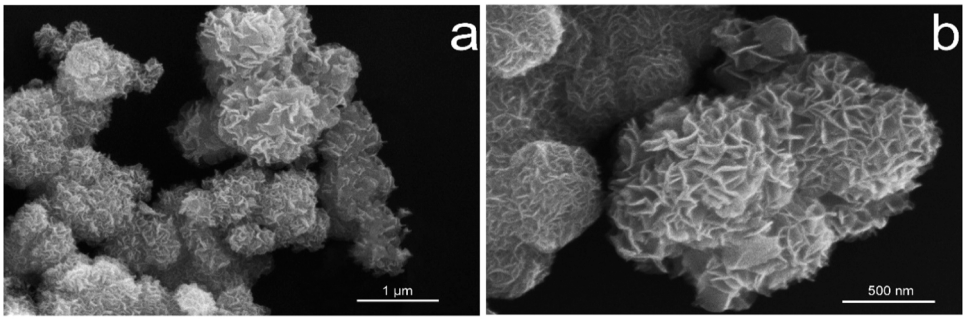

Fig. 2. FESEM images of MoS_2/LaF_3 nanoflowers.

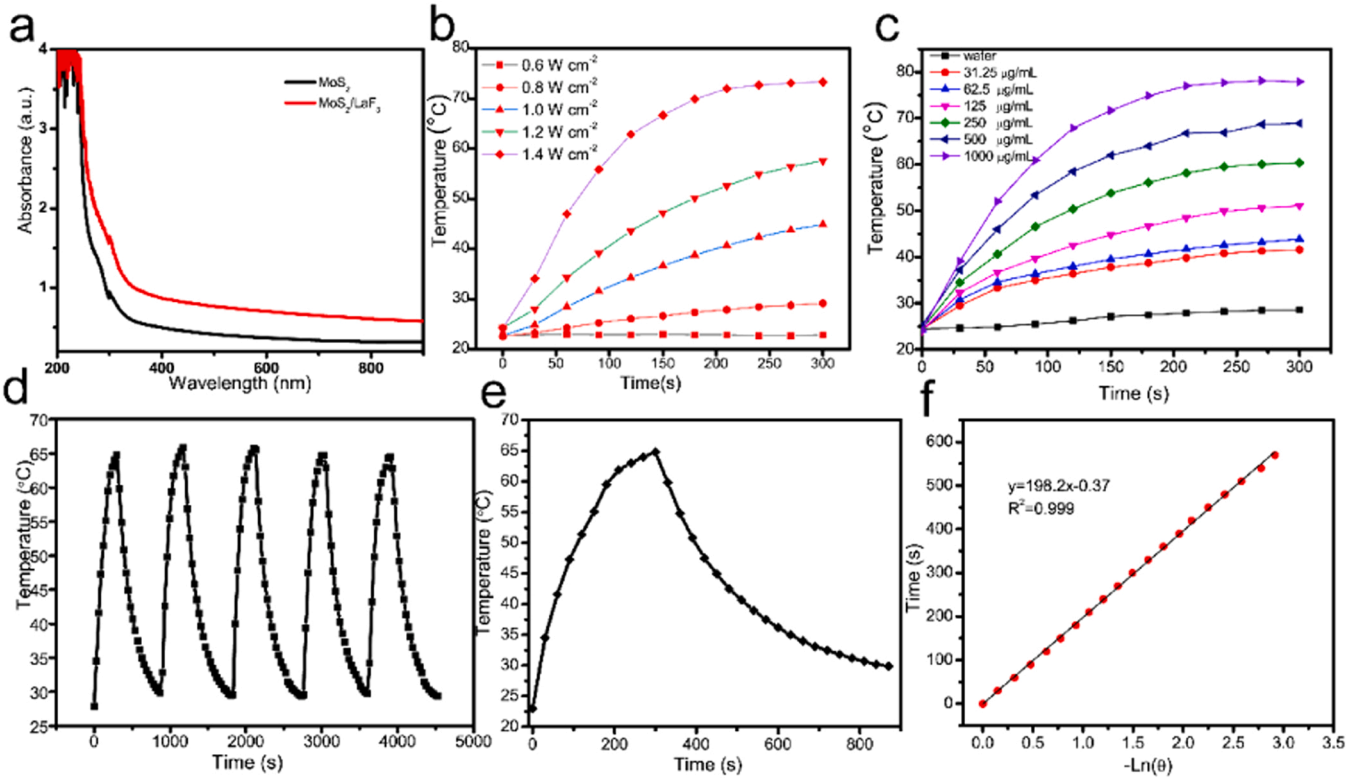

Fig. 3. (a) UV–vis spectra of MoS_2 and MoS_2/LaF_3. (b) Temperature elevation profiles of MoS_2/LaF_3 nanoflowers (500 μg mL^{-1}) with different power density (0.6–1.4 W cm^{-2}). (c) Temperature elevation profiles of MoS_2/LaF_3 nanoflowers with different concentrations (31.25–1000 μg mL^{-1}) under irradiation of 808 nm laser (1.2 W cm^{-2}) for 300 s (d) The photothermal stability of MoS_2/LaF_3 nanoflowers (500 μg mL^{-1}) over five ON/OFF cycles under irradiation of 808 nm laser (1.2 W cm^{-2}, 300 s), followed by natural cooling. (e) Photothermal effect of MoS_2/LaF_3 nanoflowers (500 μg mL^{-1}) under NIR irradiation (808 nm, 1.2 W cm^{-2}) for 300 s and natural cooling. (f) The time constant for heat transfer of MoS_2/LaF_3 nanoflowers obtained cooling time from (c).

from 41.6 °C to 77.9 °C after 300 s laser exposure, the results revealed a concentration-dependent temperature increase (Fig. 3c). The photostability of MoS_2/LaF_3 nanoflowers (500 μg/mL) was also studied during five cycles (1.2 W cm^{-2}) NIR laser irradiation. Almost no appreciable temperature change could be observed in Fig. 3d. The photostability result confirmed that the MoS_2/LaF_3 nanoflowers possessed good photothermal stability and were suitable for phototherapy *in vitro* and *in vivo*. To calculate PCE, the MoS_2/LaF_3 nanoflowers (250 μg/mL) was evaluated by measuring the temperature under NIR laser, depicted in Figs. 3e-3f. By the method reported by Roper [35], PCE (η) of MoS_2/LaF_3 nanoflowers was calculated as 342.5%. The comparison of the temperature change curve in the same situation, MoS_2/LaF_3 nanoflowers showed higher PTT effects *in vitro* (Fig. S3). When the proportion of LaF_3 further increased, the PCE was improved, it suggested that the amount of LaF_3 regulated MoS_2-based nanocomposite PTT effects (Fig. S4). Previous studies showed that 27.8% of PCE for single layered MoS_2 nanosheets [36] and 37.5% for MoS_2 nanoparticle [37]. MoS_2 acted as a material for biomedical applications. However, the high surface energy of a few layers of nanosheets tend to inevitably stack and aggregate, which limits the application severely. LaF_3 decrease interface electron scatting and increase high electron mobility, meanwhile, LaF_3 nanoparticles binding on surface of MoS_2 nanosheets improved the MoS_2 nanosheets colloidal stability and biocompatibility. Consequently, MoS_2/LaF_3 nanoflowers can quickly reach a higher temperature at low dose in a short time, thus can induce tumor cells death while minimizing damage to healthy cells.

3.3. Photothermal effect assay in vitro

The cell viability is an indispensable requirement for MoS_2/LaF_3 nanoflowers photothermal therapy. Hela, human cervical cancer cells, was used to access the safety and efficacy of PTAs *in vitro* antitumor. The

MTT assay was used to quantify tumor cell proliferation ability. Compared with control group (blue and green), MoS_2/LaF_3 nanoflowers with NIR group exhibited killing tumor cell (Fig. 4a). It was noted that MoS_2/LaF_3 nanoflowers with NIR at 250 μg/mL inhibited tumor cell viability significantly. Meanwhile, from Fig. 4a, even concentration as high as 1000 μg/mL and the cell viability of MoS_2/LaF_3 nanoflowers group maintained around 95%. The cell viability showed no apparent change with increasing MoS_2/LaF_3 nanoflowers concentrations without NIR. MoS_2/LaF_3 nanoflowers hence appeared to be very biocompatible. It is necessary to investigate the hemocompatibility of MoS_2/LaF_3 nanoflowers. Before the test *in vivo*, we needed to confirm the blood cell compatibility of MoS_2/LaF_3 nanoflowers by suspending RBCs in different concentrations of the nanocomposite. From Fig. 4b, no deposition of undamaged cells could be found in the water-treated sample after centrifugation, except for hemoglobin releasing from the damaged cells into the water. In contrast, the MoS_2/LaF_3 nanoflowers treated samples exhibited the precipitation of red cells without obvious hemolytic phenomenon occurring. The hemolysis ratio of MoS_2/LaF_3 nanoflowers was less than 5%, further implying MoS_2/LaF_3 nanoflowers had excellent compatibility. Low cytotoxicity and good blood compatibility *in vitro* allowed MoS_2/LaF_3 nanoflowers to test *in vitro*. We also explored the capability of the MoS_2/LaF_3 nanoflowers in photothermal effects on killing tumor cell. Fluorescence imaging was conducted to test the PTT effects *in vitro*. Hela cells were co-labeled with Calcein-AM/PI. This permitted us to identify between dead cells (red) and live cells (green). In addition, the early stage of apoptosis cells showed yellow fluorescence(Fig. 4c). Live cells were significantly found in PBS groups, MoS_2 and MoS_2/LaF_3 nanoflowers without NIR irradiation. Cells treated with MoS_2 showed a small amounts of cell death, surrounded by the early stage of apoptosis cells and living cells. The results suggested that the photothermal effect of MoS_2 alone could not completely kill those cells under this condition. The reason could be attributed to the lower PCE (η) of the MoS_2 (Fig. S4). In comparision, the highest number of dead tumor cells was observed at 250 μg/mL of MoS_2/LaF_3 nanoflowers with NIR laser irradiation treatment (Fig. 4c). These *in vitro* results suggested that the improvement of photothermal therapy MoS_2 decorated with LaF_3 was better and would be benefits for PTT *in vivo*.

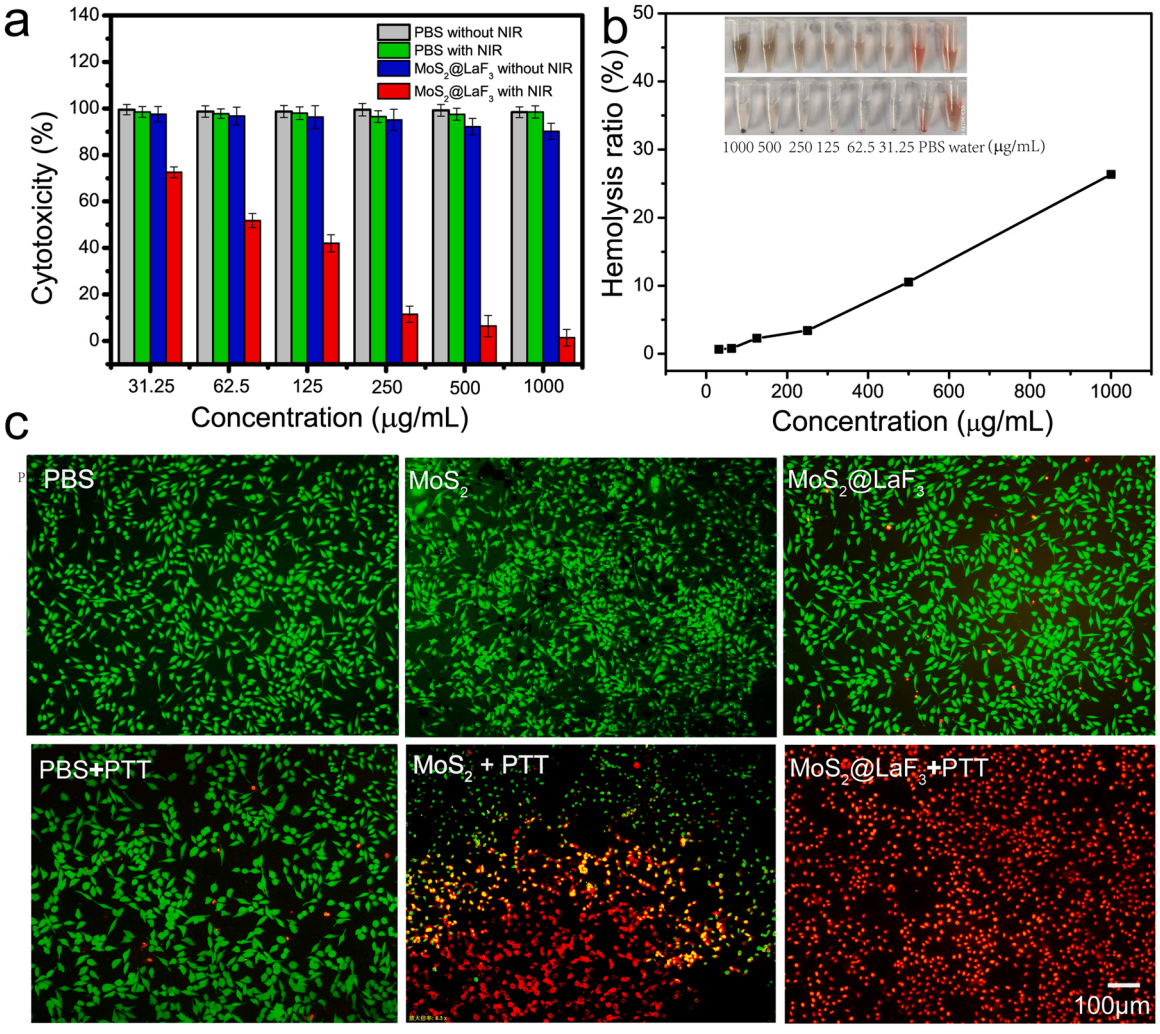

Fig. 4. (a) The cytotoxicity of Hela cells treated with various concentrations of MoS_2/LaF_3 nanoflowers; PBS NIR irradiation and the negative control of MoS_2/LaF_3 nanoflowers without NIR. Results in triplicate ± standard deviation. (b) Hemolysis test. RBCs treated with MoS_2/LaF_3 nanoflowers at different concentrations for 3 h, using DI water as negative control and PBS as the positive control. Inset: Observation Photos for of hemolysis tests comparition without centrifugation(up) and with centrifugation (down) (c) Fluorescence imaging of Hela cells incubated with 250 μg mL^{-1} of MoS_2/LaF_3 nanoflowers, MoS_2 and PBS respectively, for 4 h, irradiation of the laser (808 nm, 1.2 W cm^{-2}) for 300 s, without irradiation (up) and with irradiation (down). The cells were detected with calcein-AM/PI kit. Live cells (green fluorescence) and dead cells (red fluorescence) scale bar: 100 μm test. (For interpretation of the references to colour in this figure legend, the reader is referred to the web version of this article.)

3.4. Photothermal antitumor therapy in vivo

H22 (hepatocellular carcinomacell) is mice grafted tumor cell lines and widely applied to make the mouse tumor models for screening anticancer drugs *in vivo*. As we know, BALB/c are usually used as grafted mice tumor model for further photothermal effect study *in vivo*. Once tumor volume was ~350 mm^3, BALB/c mice were divided into four groups, female BALB/c mice were injected subcutaneously with PBS, PBS with NIR irradiation, MoS_2/LaF_3 nanoflowers and MoS_2/LaF_3 nanoflowers with NIR irradiation (808 nm, 1.2 W cm^{-2}). Compared with intravenous injection, the subcutaneous injection of nanoparticle is prone to a relative decrease in toxicity that correlate to inflammatory responses. Tumors were irradiated for only 10 min after PBS or MoS_2/LaF_3 nanoflowers injection. Accordingly, the temperatures were simultaneously recorded by the Fluke thermography camera (Fig. 5a). For the MoS_2/LaF_3 nanoflowers group treated with NIR irradiation, the temperature in the tumor site reached 62.5 °C (Fig. 5b), which was sufficient to induce enough heat to kill the tumor cell. *In vitro* experiments, the effect of MoS_2 photothermal killing on H22 cells was not obvious, and there were still many live H22 cells remaining after NIR irradiation (Fig. 4c). Therefore, MoS_2 group was not been established for *in vivo* experiments, and the investigation of photothermal effect in mice was mainly focused on MoS_2/LaF_3. Correspondingly, PBS without NIR group, PBS with NIR group, MoS_2 without NIR group, and MoS_2 with NIR group were established in the tumor inhibition experiment. Thus, mice treated with PBS, PBS with NIR, and MoS_2/LaF_3 nanoflowers groups displayed a rapid tumor-growth; for the mice treated MoS_2/LaF_3 nanoflowers with NIR, the proliferation of tumors were inhibited (Fig. 5d). It is worth mentioning, body weights of all the groups at 14 days did not show any detectable change, which proved that the MoS_2/LaF_3 nanoflowers did not induce acute toxic effects (Fig. 5c). The results were consistent with the *in vitro* cytotoxicity and hemolysis assay (Figs. 4a-4b). The tumors excised from mice were photographed (Fig. 5e). The tumors size of MoS_2/LaF_3 nanoflowers group with NIR irradiation were smaller than those of other treatment groups (Fig. 5e). These results suggested the PTT effect of MoS_2/LaF_3 nanoflowers are sufficient to eradicate the tumor cell and inhibit tumor growth.

3.5. Histopathology study

To investigate the toxicity of photothermal agent *in vivo*, major organs of the mice were isolated and stained by H&E. Compared with PBS with NIR, and MoS_2/LaF_3 nanoflowers with NIR, there were no significant histopathological damages detected in the liver, spleen, heart, kidney, and lung (Fig. 6). In additon, MoS_2/LaF_3 *in vitro* (Figs. 4a-4b) and *in vivo* test results (Fig. 5c) showed good biocompatibility. These findings demonstrated that the MoS_2/LaF_3 nanoflowers have good biocompatibility and safety for photothermal cancer therapy.

In previous work, it was found that the surface temperature of 13.09 mg cm^{-1} MoS_2/LaF_3/PDMS assembled membrane could increase

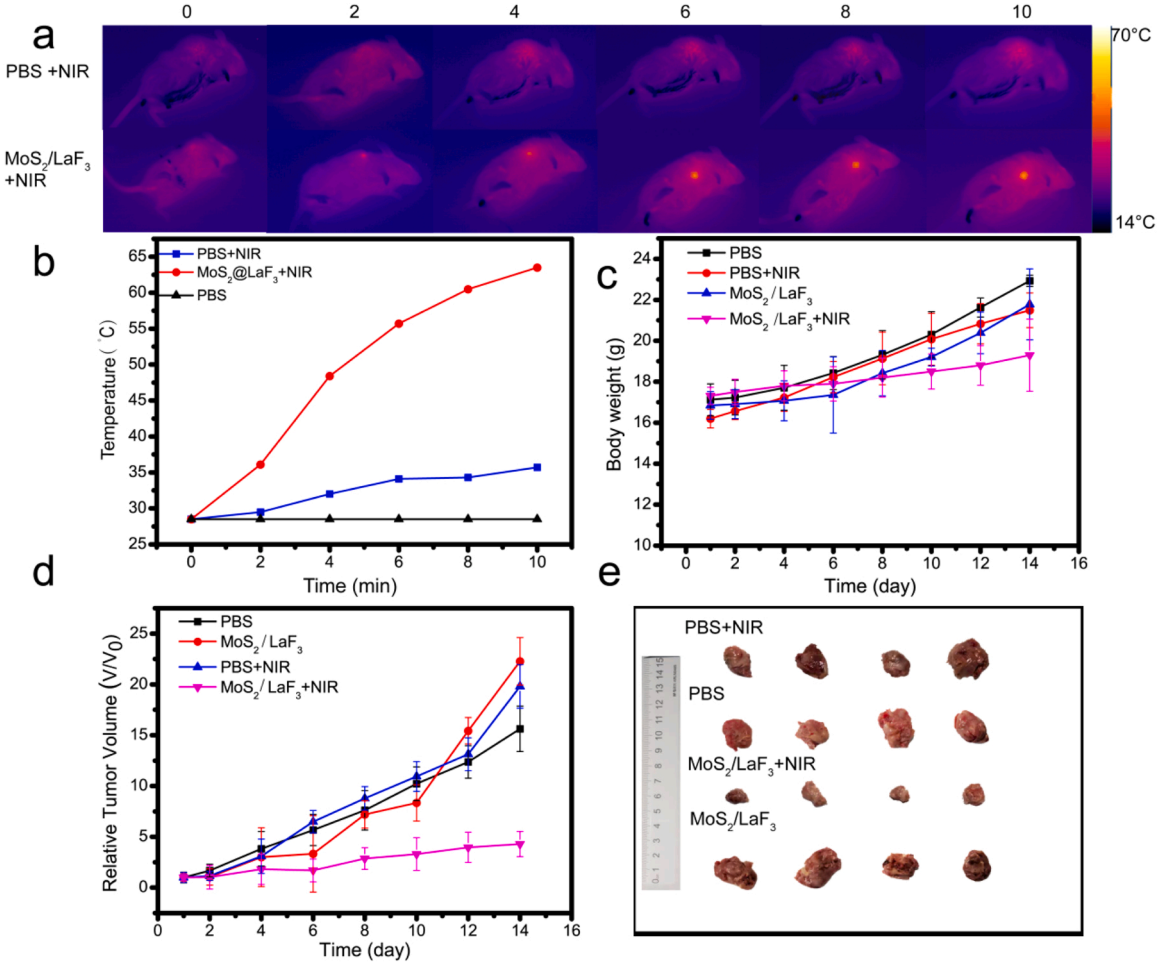

Fig. 5. (a) In *vivo* MoS_2/LaF_3 nanoflowers for photothermal therapy of cancer. Tumor-bearing mice treated with PBS, MoS_2/LaF_3 nanoflowers, respectively. Tumor temperature was monitored under the 808 nm NIR (1.2 W cm^{-2}, 10 min) (b) Corresponding temperature change (c) Body weights of tumor-bearing mice after treatment. Data were recorded as the mean ± SD (n = 4) (d) Tumor growth inhibition of mice after phototherapy treatments (e) The photos of isolated tumors from mice at the end of test.

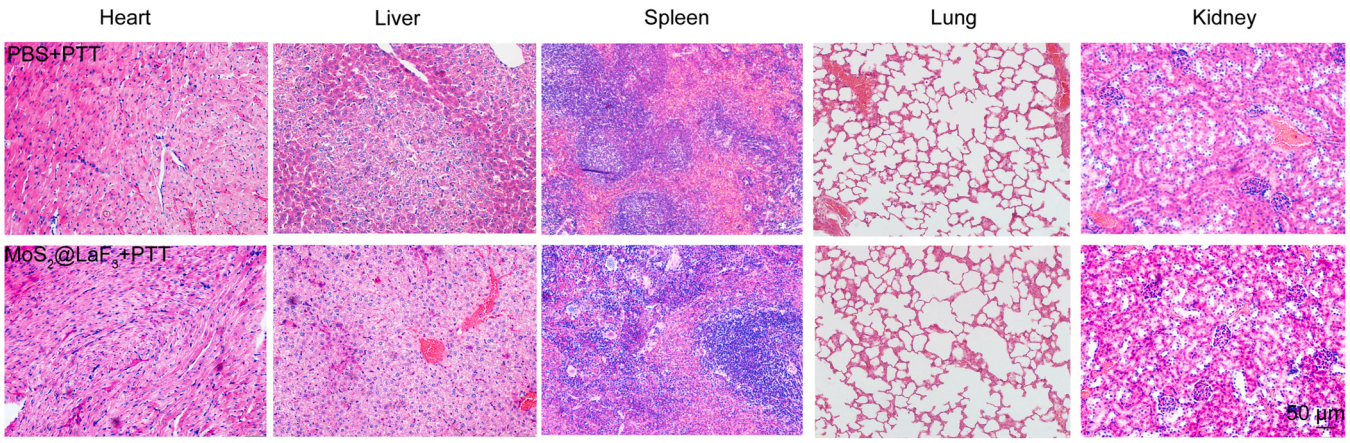

Fig. 6. Histological images of organs from mice treated with PBS+NIR and MoS_2 /LaF_3 +NIR after PTT.

by 28°C in comparision with commercial polytetrafluoroethylene membrane under light condition and sunlight, MoS_2/LaF_3/PDMS displayed high efficiency in evaporation rate and conversion efficiency [32]. Based on these photothermal effects property and application, we further applied the MoS_2/LaF_3 in treating tumor. Both *In vitro* and *in vivo* results showed the MoS_2/LaF_3 had higher heating conversion potential, the H22, the poor differentiated hepatoma was effectively destroyed. The tumor growth significantly inhibited. This work provided a new efficient MoS_2-based-PTT strategy with high photothermal therapeutic efficacy.

4. Conclusions

In summary, we had successfully prepared MoS_2/LaF_3 nanoflowers, which was based on LaF_3 nanoparticle modified with MoS_2 assembly, good water solubility and high photothermal effect for cancer therapy. MoS_2/LaF_3 nanoflowers also exhibited good stability and compatibility in biological environment. The MoS_2/LaF_3 nanoflowers with 42.5% PCE can efficiently convert the absorbed NIR to hyperthermia. The safe and effective cytotoxicity *in vitro* achieved by PTT was observed, indicating that LaF3 improve the MoS_2-based phototherapy. Due to the enhanced PTT in the H22 hepatocellular tumor model, the significant cancer treatment effect was also observed *in vivo* tumor growth inhibition therapy. Overall, our results not only provided a potential PTT therapy platform, also promoted to research on other nanomaterials with better performance for antitumor therapy.

CRediT authorship contribution statement

Xuelin Wang: Supervision, Funding acquisition. **Lin Sun:** Writing – original draft, Writing – review & editing. **Huifang Bai and Weidong Qiao:** Design and execute animal experiment. **Hanjin Jiang:** Methodology, Data curation, Formal analysis. **Peng Zhang and Jian Li:** Visualization, Investigation. **Dong Wang:** Formal analysis, Data curation. **GuoSong Liu:** Writing – review & editing.

Declaration of Competing Interest

The authors declare that they have no known competing financial interests or personal relationships that could have appeared to influence the work reported in this paper.

Acknowledgement

The authors acknowledge the financial support by the National Key R&D Program of China (2018YFC1602500), National Natural Science Foundation of China (Grant No.51602123).

Appendix A. Supporting information

Supplementary data associated with this article can be found in the online version at doi:10.1016/j.colsurfb.2022.112462.

References

[1] G.L. Semenza, Targeting HIF-1 for cancer therapy, Nat. Rev. Cancer 3 (2003) 721–732, https://doi.org/10.1038/nrc1187.
[2] Y. Cao, J.M. Eble, E. Moon, H. Yuan, D.H. Weitzel, C.D. Landon, C.Y. Nien, G. Hanna, J.N. Rich, J.M. Provenzale, M.W. Dewhirst, Tumor cells upregulate normoxic HIF-1α in response to doxorubicin, Cancer Res. 73 (2013) 6230–6242, https://doi.org/10.1158/0008-5472.can-12-1345.
[3] J.R. Muindi, Retinoids in clinical cancer therapy, Cancer Treat. Res. 87 (1996) 305–342, https://doi.org/10.1007/978-1-4613-1267-3_13.
[4] N. Girard, Antiangiogenic agents and chemotherapy in advanced non-small cell lung cancer: a clinical perspective, Expert Rev. Anticancer Ther. 13 (2013) 1193–1206, https://doi.org/10.1586/14737140.2013.845093.
[5] Z. Du, K. Yan, Y. Cao, Y. Li, Y. Yao, G. Yang, Regenerated keratin-encapsulated gold nanorods for chemo-photothermal synergistic therapy, Mater. Sci. Eng. C. Mater. Biol. Appl. 117 (2020), 111340, https://doi.org/10.1016/j.msec.2020.111340.
[6] G. Farahavar, S.S. Abolmaali, F. Nejatollahi, A. Safaie, S. Javanmardi, H. Khajeh Zadeh, R. Yousefi, H. Nadgaran, S. Mohammadi-Samani, A.M. Tamaddon, S. Ahadian, Single-chain antibody-decorated Au nanocages@liposomal layer nanoprobes for targeted SERS imaging and remote-controlled photothermal therapy of melanoma cancer cells, Mater. Sci. Eng. C. Mater. Biol. Appl. 124 (2021), 112086, https://doi.org/10.1016/j.msec.2021.112086.
[7] X. Zhan, W. Teng, K. Sun, J. He, J. Yang, J. Tian, X. Huang, L. Zhou, C. Zhou, CD47-mediated DTIC-loaded chitosan oligosaccharide-grafted nGO for synergistic chemo-photothermal therapy against malignant melanoma, Mater. Sci. Eng. C. Mater. Biol. Appl. 123 (2021), 112014, https://doi.org/10.1016/j.msec.2021.112014.
[8] L. Sun, Y. Shi, M. Tang, D. Wang, Y. Tian, J. Li, Facile synthesis of urchin-like LaWO(4)Cl assemblies and their near-infrared photothermal conversion, Nanoscale 11 (2019) 14237–14241, https://doi.org/10.1039/c9nr03082d.
[9] M.C. Wu, A.R. Deokar, J.H. Liao, P.Y. Shih, Y.C. Ling, Graphene-based photothermal agent for rapid and effective killing of bacteria, ACS Nano 7 (2013) 1281–1290, https://doi.org/10.1021/nn304782d.
[10] Z. Zhao, G. Jia, Y. Liu, Q. Zhang, N. Wang, Microwave-assisted synthesis and photothermal conversion of Cu2 – xSe hollow structure, J. Nanopart. Res. 21 (2019) 47, https://doi.org/10.1007/s11051-019-4489-2.
[11] Q. Hu, Z. Huang, Y. Duan, Z. Fu, L. Bin, Reprogramming tumor microenvironment with photothermal therapy, Bioconjug Chem. 31 (2020) 1268–1278, https://doi.org/10.1021/acs.bioconjchem.0c00135.
[12] X. Fu, H. Bai, F. Lyu, L. Liu, S. Wang, Conjugated polymer nanomaterials for phototherapy of cancer, Chem. Res. Chin. Univ. 36 (2020) 237–242, https://doi.org/10.1007/s40242-020-0012-7.
[13] J. Xu, L. Wu, P. Yu, M. Liu, Y. Lu, Effect of two recombinant Trichinella spiralis serine protease inhibitors on TNBS-induced experimental colitis of mice, Clin. Exp. Immunol. 194 (2018) 400–413, https://doi.org/10.1111/cei.13199.
[14] F. Pierini, P. Nakielski, O. Urbanek, S. Pawłowska, M. Lanzi, L. De Sio, T. A. Kowalewski, Polymer-based nanomaterials for photothermal therapy: from light-responsive to multifunctional nanoplatforms for synergistically combined technologies, Biomacromolecules 19 (2018) 4147–4167, https://doi.org/10.1021/acs.biomac.8b01138.
[15] F. Pierini, A. Guglielmelli, O. Urbanek, P. Nakielski, L. Pezzi, R. Buda, M. Lanzi, T. A. Kowalewski, L. De Sio, Thermoplasmonic-activated hydrogel based dynamic light attenuator, Adv. Opt. Mater. 8 (2020), 2000324, https://doi.org/10.1002/adom.202000324.

[16] X. Meng, Z. Liu, Y. Cao, W. Dai, K. Zhang, H. Dong, X. Feng, X. Zhang, Fabricating aptamer-conjugated PEGylated-MoS2/Cu1.8S theranostic nanoplatform for multiplexed imaging diagnosis and chemo-photothermal therapy of cancer, Adv. Funct. Mater. 27 (2017), 1605592, https://doi.org/10.1002/adfm.201605592.
[17] A. Zhang, A. Li, W. Zhao, G. Yan, B. Liu, M. Liu, M. Li, B. Huo, J. Liu, An efficient and self-guided chemo-photothermal drug loading system based on copolymer and transferrin decorated MoS2 nanodots for dually controlled drug release, Chem. Eng. J. 342 (2018) 120–132, https://doi.org/10.1016/j.cej.2018.02.081.
[18] Y.R. Lim, Y.B. Lee, S.K. Kim, S.J. Kim, Y. Kim, C. Jeon, W. Song, S. Myung, S.S. Lee, K.-S. An, J. Lim, Rational design of multifunctional devices based on molybdenum disulfide and graphene hybrid nanostructures, Appl. Surf. Sci. 392 (2017) 557–561, https://doi.org/10.1016/j.apsusc.2016.09.082.
[19] S. Ariyasu, J. Mu, X. Zhang, Y. Huang, E.K.L. Yeow, H. Zhang, B. Xing, Investigation of thermally induced cellular ablation and heat response triggered by planar MoS(2)-based nanocomposite, Bioconjug Chem. 28 (2017) 1059–1067, https://doi.org/10.1021/acs.bioconjchem.6b00741.
[20] A. Albu-Yaron, M. Levy, R. Tenne, R. Popovitz-Biro, M. Weidenbach, M. Bar-Sadan, L. Houben, A.N. Enyashin, G. Seifert, D. Feuermann, E.A. Katz, J.M. Gordon, MoS2 hybrid nanostructures: from octahedral to quasi-spherical shells within individual nanoparticles, Angew. Chem. Int Ed. Engl. 50 (2011) 1810–1814, https://doi.org/10.1002/anie.201006719.
[21] S. Wang, K. Li, Y. Chen, H. Chen, M. Ma, J. Feng, Q. Zhao, J. Shi, Biocompatible PEGylated MoS2 nanosheets: controllable bottom-up synthesis and highly efficient photothermal regression of tumor, Biomaterials 39 (2015) 206–217, https://doi.org/10.1016/j.biomaterials.2014.11.009.
[22] G. Guan, S. Liu, Y. Cheng, Y.W. Zhang, M.Y. Han, BSA-caged metal clusters to exfoliate MoS(2) nanosheets towards their hybridized functionalization, Nanoscale 10 (2018) 10911–10917, https://doi.org/10.1039/c8nr02121j.
[23] C. Li, E. Mei, C. Chen, Y. Li, B. Nugasur, L. Hou, X. Ding, M. Hu, Y. Zhang, Z. Su, J. Lin, Y. Yang, P. Huang, Z. Li, Gold-nanobipyramid-based nanotheranostics for dual-modality imaging-guided phototherapy, ACS Appl. Mater. Interfaces 12 (2020) 12541–12548, https://doi.org/10.1021/acsami.0c00112.
[24] J. Ge, E.C. Ou, R.Q. Yu, X. Chu, A novel aptameric nanobiosensor based on the self-assembled DNA-MoS(2) nanosheet architecture for biomolecule detection, J. Mater. Chem. B 2 (2014) 625–628, https://doi.org/10.1039/c3tb21570a.
[25] M.Y. Peng, D.W. Zheng, S.B. Wang, S.X. Cheng, X.Z. Zhang, Multifunctional nanosystem for synergistic tumor therapy delivered by two-dimensional MoS(2), ACS Appl. Mater. Interfaces 9 (2017) 13965–13975, https://doi.org/10.1021/acsami.7b03276.
[26] S. Begum, A. Pramanik, K. Gates, Y. Gao, P. Ray, Antimicrobial-peptide-conjugated mos2 based nanoplatform for multimodal synergistic inactivation of superbugs, ACS Appl. Bio Mater. 2 (2018), https://doi.org/10.1021/acsabm.8b00632.
[27] K. Zhou, J. Liu, W. Zeng, Y. Hu, Z. Gui, In situ synthesis, morphology, and fundamental properties of polymer/MoS2 nanocomposites, Compos. Sci. Technol. 107 (2015) 120–128, https://doi.org/10.1016/j.compscitech.2014.11.017.
[28] X. Dong, W. Yin, X. Zhang, S. Zhu, X. He, J. Yu, J. Xie, Z. Guo, L. Yan, X. Liu, Q. Wang, Z. Gu, Y. Zhao, Intelligent MoS(2) nanotheranostic for targeted and enzyme-/pH-/NIR-responsive drug delivery to overcome cancer chemotherapy resistance guided by PET imaging, ACS Appl. Mater. Interfaces 10 (2018) 4271–4284, https://doi.org/10.1021/acsami.7b17506.
[29] Y. Liu, J. Liu, Hybrid nanomaterials of WS(2) or MoS(2) nanosheets with liposomes: biointerfaces and multiplexed drug delivery, Nanoscale 9 (2017) 13187–13194, https://doi.org/10.1039/c7nr04199c.
[30] Y. Yang, B. Gong, Y. Yang, A. Xie, Y. Shen, M. Zhu, Construction and synergistic anticancer efficacy of magnetic targeting cabbage-like Fe(3)O(4)@MoS(2)@ZnO drug carriers, J. Mater. Chem. B 6 (2018) 3792–3799, https://doi.org/10.1039/c8tb00608c.
[31] Y. Zhao, G. Deng, X. Liu, L. Sun, H. Li, Q. Cheng, K. Xi, D. Xu, MoS2/Ag nanohybrid: a novel matrix with synergistic effect for small molecule drugs analysis by negative-ion matrix-assisted laser desorption/ionization time-of-flight mass spectrometry, Anal. Chim. Acta 937 (2016) 87–95, https://doi.org/10.1016/j.aca.2016.06.026.
[32] H. Jiang, H. Fang, D. Wang, J. Sun, Spray-coated commercial PTFE membrane from MoS2/LaF3/PDMS ink as solar absorber for efficient solar steam generation, Sol. RRL 4 (2020), 2000126, https://doi.org/10.1002/solr.202000126.
[33] J. Huang, L. Ye, X. Gao, H. Li, J. Xu, Z. Li, Molybdenum disulfide-based amplified fluorescence DNA detection using hybridization chain reactions, J. Mater. Chem. B 3 (2015) 2395–2401, https://doi.org/10.1039/c4tb01986e.
[34] H. Li, Q. Zhang, C.C.R. Yap, B.K. Tay, T.H.T. Edwin, A. Olivier, D. Baillargeat, From bulk to monolayer MoS2: evolution of Raman scattering, Adv. Funct. Mater. 22 (2012) 1385–1390, https://doi.org/10.1002/adfm.201102111.
[35] D.K. Roper, W. Ahn, M. Hoepfner, Microscale heat transfer transduced by surface plasmon resonant gold nanoparticles, J. Phys. Chem. C. Nanomater Interfaces 111 (2007) 3636–3641, https://doi.org/10.1021/jp064341w.
[36] J. Liu, J. Zheng, H. Nie, D. Zhang, D. Cao, Z. Xing, B. Li, L. Jia, Molybdenum disulfide-based hyaluronic acid-guided multifunctional theranostic nanoplatform for magnetic resonance imaging and synergetic chemo-photothermal therapy, J. Colloid Interface Sci. 548 (2019) 131–144, https://doi.org/10.1016/j.jcis.2019.04.022.
[37] H. Yang, J. Zhao, C. Wu, C. Ye, D. Zou, S. Wang, Facile synthesis of colloidal stable MoS2 nanoparticles for combined tumor therapy, Chem. Eng. J. 351 (2018) 548–558, https://doi.org/10.1016/j.cej.2018.06.100.